Imperial College London

Department of AERONAUTICS

# Pipe Flow Lab Report

Dhruva Teja Turaga

CID: 02385740

**Abstract**

This report presents a comprehensive comparison of experimental, computational, and theoretical methods for analysing flow through a pipe, with a focus on predicting the skin friction coefficients for different Reynolds numbers. The experimental procedure involved direct measurement of pressure difference along different positions of the pipe, providing precise data but subject to experimental uncertainties. Computational fluid dynamics (CFD) methods offer detailed simulations of flow behavior, providing skin friction coefficient predictions across various conditions, albeit with computational resource demands. The software used in this report is STAR CCM by SIEMENS as it has both graphing and visual representational capabilities. Theoretical models, derived from fundamental fluid mechanics principles, offer analytical expressions for estimating skin friction coefficients based on simplified flow assumptions, providing quick estimates but potentially lacking accuracy in complex scenarios. By synthesising results from all three methods, a more comprehensive understanding of pipe flow dynamics and skin friction coefficients can be achieved, enhancing engineering design and analysis capabilities. The standards used within the experiment and CFD are BS-EN ISO 81060-1:2012 and ISO 16730-1 respectively. Additionally, the experimental data recieved can be read through using appendix C and all graphs shown within this report are created in MATLAB in which the code can be accessed using appendix D.

December 16, 2024

# Contents

# List of Tables

# List of Figures

# Nomenclature

| | |
|---|---|
| $\Delta h_0$ | Difference in manometer readings across the orifice plate (m) |
| $\Delta p_0$ | Pressure across the orifice plate (kg$m^{-1}s^{-2}$) |
| $\mu_{air}$ | Dynamic viscosity of air (kg$m^{-1}s^{-1}$) |
| $\rho_a, \rho_m$ | Density of air, Density of alcohol inside manometer (kg $m^{-3}$) |
| $\tau_w$ | Shear stress at wall (kg$m^{-1}s^{-2}$) |
| $\theta$ | Inclination of manometer ($\circ$) |
| $C_f$ | Skin Friction Coefficient ($\circ$) |
| $D$ | Pipe Diameter (m) |
| $g$ | acceleration due to gravity (m$s^{-1}$) |
| $h_n$ | Manometer reading for the $n^{th}$ static tapping (m) |
| $h_{01}$,$h_{02}$ | Manometer readings for each side of the orifice plate (m) |
| $k$ | Orifice calibration factor |
| $p$ | Pressure (kg$m^{-1}s^{-2}$) |
| $Re_D$ | Reynolds Number based on pipe diameter and bulk velocity |
| $V$,$V_\infty$ | Mean/Bulk Velocity, Free stream Velocity in pipe (m$s^{-1}$) |
| $x$ | Distance from first tapping (m) |

# 1 Introduction

Within engineering the effects of solid walls on fluid flow around objects play an important role in dictating how the properties of the fluid in motion change radially as you go closer to the wall and progression of the flow as it matures. Pipe flow introduces a range of engineering problems, including energy losses in the fluid caused by friction with the pipe walls, leading to a gradual decline in pressure along the pipeline. Additionally, turbulence exacerbates these frictional losses, causing pressure fluctuations throughout the entire length of the pipe, which is an issue as pipes are used in many real world applications from the flow of blood in blood vessels to effects of skin-friction drag on a fuselage as objects moving through fluids exhibit the same properties as fluids moving past objects.[1] Therefore, it is important to model the flow of fluids, taking into account the disadvantages from accuracy of the models to validation which is challenging without robust experimental data and limitations of computational power.

In this experiment the main question we aim to answer is how does fluid mature as it develops through the pipe both along the length and from the centre line to the wall. Breaking this down, specifically, we aim to determine the region in which the flow transitions from laminar to turbulent as well as calculate the Reynolds number at the different velocities along with identifying how the velocity and pressure coefficient varies radially and along the pipe. Finally, investigate how the skin friction varies experimentally, theoretically and computationally to assess the accuracy of all the three methods in predicting flow parameters.

The study of boundary layer, specifically, plays an important role in even aspects of our civilization, for example, in building construction, since humans live in 'Earth's own boundary layer'. The Boundary Layer is a region in the movement of flow over an object as it is where the average fluid velocity decreases from the free stream value $V_\infty$ to zero. The variation in velocity between laminar and turbulent within the boundary layer which results in a shear stress that dissipates fluid momentum causes drag.[2] In a laminar flow, the shear is the variation of velocity from zero, at the wall, to a finite value $V_\infty$ in the free stream, which occurs due to random motion of fluids superposed on the continuum flow field. These shear stresses are relatively small compared to those developed in turbulent flows, but come from the random three dimensional chaotic movement of large packets of fluid, over a range of sizes.[3] Although systematic studies were only first performed in the $20^{th}$ century, the practical importance led to studies also dating back to the late $18^{th}$ century by the works of Chézy.[4] In 1883, Osborne Reynolds first investigated the transition of laminar to turbulent flow within a pipe by increasing the velocity, therefore increasing the Reynolds number. By adding a dye and following the path he observed the path changed into a more chaotic motion as velocity increases.[5]

The experimental method by Reynolds is a good alternative ways to model flow and observe the exact point at which the flow is fully developed unlike the use of manometers in this experiment. The analysis of the data has been done by many scientists in different forms and using different quantities to calculate $C_f$. Hagen and Poiseuille measured the flow rates and pressure drops in laminar pipes to balance the driving force to the shear stress on walls to obtain their approximate to $C_f$ using their empirical evidence which correlated very closely to theoretical values.[6] From another stand point, Nikuradse used sand roughened pipes and water of varying pressure to measure the pressure drops and calculate the pressure differential.[7] From correlating the friction factor to Reynolds number it is possible to calculate the $C_f$ as it is a function of the Reynolds Number. Although, CFD was not used, the formulae derived from empirical data paved an effective way to compare directly to not only show the accuracy from experimental to the computational model but validity if similar experiments were reproduced by scientists who derived the formulae. Within computational fluid dynamics, the standard related would be ISO 16730-1, however, during the experiment the standards followed are BS-EN ISO 81060-1:2012 for use of manometers within the laboratory setting.

## 1.1 Methodology

The experiment was conducted using a virtual manometer and pressure tappings along the circular section of a Perspex pipe of diameter 9.5mm. The mean velocity is determined by the pressure difference across the orifice plate an as fluid passes through, the difference in pressure caused by the obstruction of the orifice plate can then be used to determine the speed of the flow. The manometer angle and height is measured approximately, due to large fluctuations and used in conjunction with a a running plot to see the trend of the data as it is recorded. The running plot equation used is stated in equation (1) and should remain stable for the laminar and steep increase once turbulent.[8]

$$\frac{\Delta h_{17}\sin(\theta)}{\sqrt{(\Delta h_0\sin(\theta))}} vs. \sqrt{(\Delta h_0\sin(\theta))} \tag{1}$$

# 2 CFD Model Setup and Verification

## 2.1 Model Setup

To model the flow of air through a pipe in three dimensions is a computationally difficult task requiring lots of processing power. However, looking at a pipe it has key characteristics we can take advantage of such as an inlet and an outlet with constant circular cross sectional area, this means we can just use the plane across the middle of the pipe. Geometrically, the plane is just the face of a cuboid of height relating to the radius which we can transform it using axisymmetry. The concept of this is shown in appendix A.
Using the planar region, we can convert out existing model into an array of cells, the mesh, of a particular size known as the base size as shown in figure 1. The flow physics occurs on each mesh cell, calculating values from the pipe's center to the wall and along its length. Specific quantities can be visualised in scalar scenes, revealing how they propagate as the flow matures. The physics can accurately compute complex flows at high speed, relying on known assumptions about the fluid and the specific pipe. By giving initial velocity, direction as well as fluid properties like segregated flow with the knowledge that it is a viscous and incompressible, the task of calculating velocity, pressure coefficient etc. at any instant in the pipe is suddenly notably less complex. The quantities used for density of air is 1.29 $kg/m^3$, assuming at sea level, the velocity based on a confident laminar $Re_D$ is 1.116 $m/s$ as well as relative pressure being zero to the atmospheric pressure.

Figure 1: Mesh of model created with base size 0.001m

## 2.2 Verification

Without experimental data, we can theoretically predict the radial velocity profile in a fully developed flow to make a direct comparison with our computation, expecting it to peak at the center and decrease parabolically to zero at the pipe wall due to the incompressible nature and constant air density. We can guarantee that the flow is fully developed from figure 2a as the velocity along the graph converges at a constant value. At this point the flow is fully evolved such that there is no further change in the fluid properties along the direction of the flow which occurred at roughly 1m with the velocity of 2.18 m/s. We can then confirm that the decrease is parabolic from statistical methods, the coefficient of regression, $R^2$, number in figure 2b shows an almost perfect shape of the given parabolic equation. Since the flow is parabolic when it is fully developed it can be expressed as equation (2) with $v_i$ as the initial velocity and $R$ as the radius of the pipe. As seen in figure 2b, the computational model closely aligns with our theoretical prediction, being along the same magnitude. To the gauge error, mesh convergence using a higher resolution base size, 6E-4, is performed and reveals it is closer to the theory and follows a perfect parabola, closer than our previous model. This presents how precise models with 8 cells compared to 4 can be and to reach a reasonable level of accuracy to theory 10 cells would give the model near exact answers without using too much more processing power.

$$\frac{u}{v_i} = 2\left(1 - \left(\frac{r}{R}\right)^2\right) \tag{2}$$

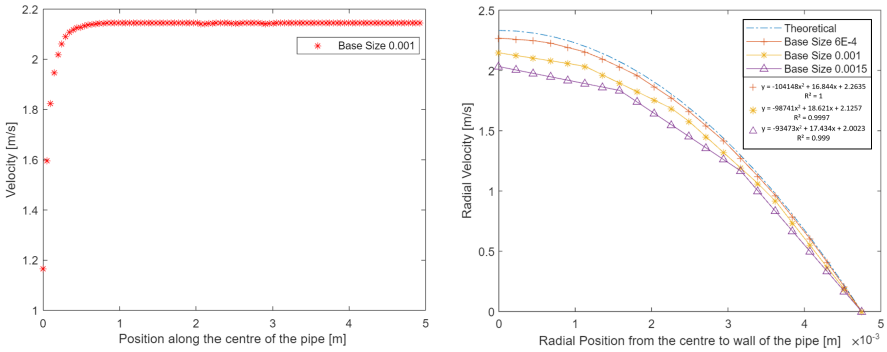


(a) Velocity along the centre of the pipe depicting fully developed nature

(b) Comparison of different CFD base sizes to the true theoretical prediction

Figure 2: Comparison of theory to CFD of full developed pipe flow

# 3 Results and Discussions

## 3.1 Computational Convergence

Within CFD the exact solution to an iterative problem is unknown but it is possible to get sufficiently close to the solution to a degree of accuracy. Residuals is one way of measuring the convergence by quantifying the error within the solutions of the system equations. As each cell within the mesh has its own approximate solution to quantities as the flow matures, it therefore has its own residual value for each of the equations solved and the normalised root mean square absolute error of the entire mesh, comparing this per iteration is the residual error shown on figure 3a. This shows past 450 iterations the error between adjacent iterations is low so the convergence starts.
The continuity residual refers to the conservation of mass within a flow simulation which states the rate of change of mass within a control volume must be equal to the net rate of mass flow into or out of the control volume shown in appendix B equation (7). The graph shows the error between the true value in satisfying the equation and the computed value is approximately 1x10$^-$4 which is the point at which the mass conservation is adequately satisfied at around 250 iterations showing no matter the time taken to compute this is the smallest error the computational model can get to the solution.
The X and Y momentum refer then to the conservation of momentum in the X and Y direction respectively as the fluid flows. Within the CFD simulation, it refers to the momentum equation, a component of the Navier-Stokes Equations, found in appendix B equation (8). The Navier-Stokes equations is the partial differential equation describing the fluid flow taking in parameters such as acceleration in the direction of flow and opposing it, the pressure forces and viscous forces. The convergence of the X-momentum to such a low error, 1x10$^-$4, indicates the high level of accuracy and stability of the computation and the model is as refined as it possibly can be even if the number of iterations is increased, this is only for the 2013 version of the software, however, the 2019 version, as shown in figure 3b, is much more accurate in computational accuracy having 1x10$^-$14 difference between adjacent values.[9]

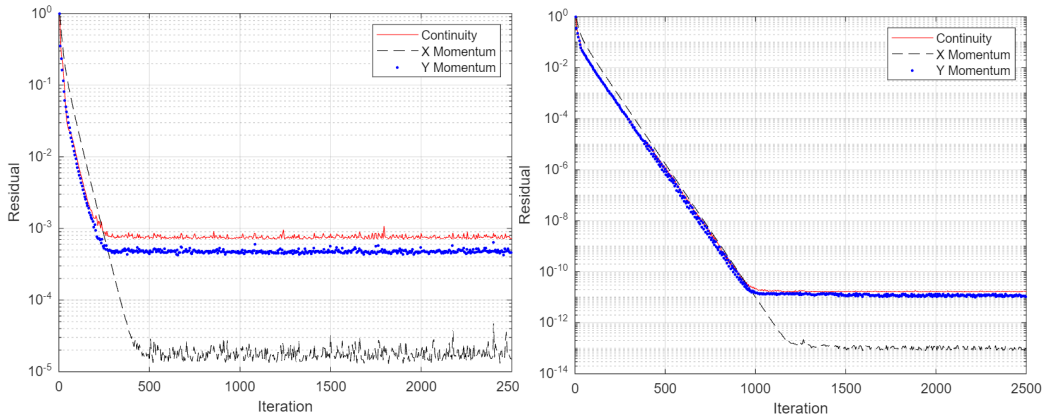


(a) STAR CCM+ 2013 Residual

(b) STAR CCM+ 2019 Residual

Figure 3: Comparison of accuracy of varying versions of CFD

## 3.2 Computational, Theoretical and Experimental Results

The $C_f$ is an important parameter within flow of any fluid over any surface as it has the function of drag associated with it. This tells us if significantly more force needs to be exerted or less to induce sliding. The $C_f$ can be expressed as equation (3).

$$C_f = \frac{\tau_w}{\frac{1}{2}\rho V^2} = f(Re_D) \tag{3}$$

With $\tau_w$ having the capability of being calculated in varies ways as in equation (4).

$$\frac{\pi D^2}{4}\frac{dp}{dx}dx = \pi D\tau_w dx \text{ or } \tau_w = \frac{D}{4}\frac{dp}{dx} = \mu\frac{du}{dy} \tag{4}$$

As shown in Table 1 at a Reynolds number of 710, in the most ideal flow situation the $C_f$ would be 0.0225,calculated from experimentally the error of 45.333% was introduced due to the unavailability of 2 manometers which decreased the measured pressure gradient causing a systematic error as the unavailable 6th and 2nd manometers play a huge role in affecting the 1st and 2nd, which were needed for the difference.

Additionally, the fluctuations of the virtual manometer prevented steady reasons adding on a certain random percentage error on each reading. Computationally, The error was much less dissimilar to the theoretical, having an error of only 1.778%. This error can only be subject to the uncertainty from the residual as the conditions were almost perfectly ideal in both ways of calculating the $C_f$. However, comparing all the values amongst each other shows, even with experimental inaccuracy, the degree is the same indicating they are all sufficiently accurate ways of calculating flow coefficients.

| Method | Cf |
|---|---|
| Theoretical | 0.0225 |
| Experimental | 0.0123 |
| Computational via pressure | 0.0221 |
| Computational via velocity | 0.0221 |

Table 1: Variation of Cf with different methods of observing fluid flow

Comparing our computational model with the experiment conducted, the general trend is a linear decrease, in the most ideal scenarios the computational model is the most accurate and true value. Experimentally,the data although close did not fit the model with great accuracy, this could be due to a multitude of factors such as parameters in CFD which we assumed to be constant but could change as flow develops such as pressure, density and temperature as well as assuming the pipe is fully smooth which has a great impact towards the pressure gradient affecting the data points. Experimentally, the pressure coefficient is calculated from the manometer readings at each tapping. As shown below in equation (5), from the distance between manometers and the orifice calibration factor the pressure coefficient points can be determined. The uncertainty between the gradients is 26.979%, primarily due to the end point, however, due to the low sample size of points and manometer holes we cannot assume with certainty whether the point is anomalous. This specific graph shows how our experimental data can be validated with a CFD model and how the plot should look if conducted in the perfect environment. The error bar calculated was from the mean of the data points, although sample size was small, it is an important factor to still consider within this experiment due to the number of uncertainties.

$$C_p = \frac{\Delta p}{\frac{1}{2}\rho V_\infty^2} = \frac{h_n - h_{01}}{k\Delta h_0} \tag{5}$$

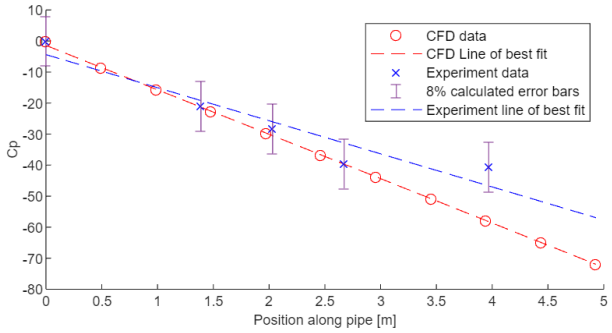


Figure 4: Variation of $C_p$ along the pipe in computational and experimental methods

### 3.3 Variation of Skin Friction Coefficient

Comparing the experimental and theoretical plots of the data. Within the laminar section of figure 5, the general trend for both theoretical and experimental is a decreasing gradient along the same magnitude. Using the formula 16 over $Re_D$, as the $Re_D$ of the flow increases, the $C_f$, skin friction coefficient, decreases which follows the pattern we expect as $Re_D$ is a function of velocity and as the velocity increases the equation can be simplified to a constant multiplied by a reciprocal velocity graph which tends towards the constant value. Representing this on a logarithmic graph of base ten it would appear as a linear graph as the decrease is not regular due to that fact that $C_f$ decreases much more as the $Re_D$ increases by a certain value. The uncertainty between the theoretical laminar and experimental laminar gradients is 70% calculated from the gradients. Although this is quite high, the laminar region of the flow is a difficult region to take accurate readings from. The magnitude of this uncertainty arises mainly from capturing readings from the manometer due to fluctuations and inaccurate scale on the virtual manometer, along with this there are factors which

don't contribute directly or greatly but can cause variation in the data such as temperature and density over a long period of time. There was one specific point which was an anomaly and discluded at (3.08,-2.06) as the error associated is much greater in order for it to fit the trend line.
Within the turbulent flow region in figure 5, the data cannot be represented as a function as it is an unknown polynomial which gets closer to the solution with the order of power. However, based on Prandtl's formula, as shown in equation (6), conducted by his experiment in 1930 on the theories for resistance along smooth plates.[10] The data fits his approximation with under 4.8% error between, this uncertainty is very minute as conditions around both experiments were around equal and since turbulent flow has more energy the ability to withstand the adverse pressure gradient doesn't change the values greatly when reproducing results. No values are anomalous however the region taken is small, in this case if conducting the experiment again, a greater range of $Re_D$ would be used to see if the trend follows for extremely high $Re_D$ and how the impact of vortices effect the flow over time.

$$\frac{1}{\sqrt{C_f}} = -0.4 + 4\log(Re\sqrt{C_f}) \tag{6}$$

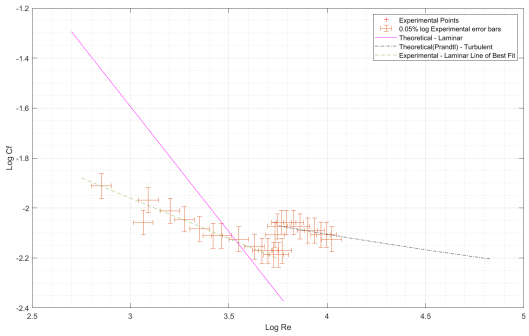


Figure 5: Variation of $C_f$ with $Re_D$ of experimental and empirical models

## 3.4 Computational Turbulent Models

As seen above, computationally modelling flow is an extremely consistent and accurate way of visualising the flow and measuring vital parameters to quantify the evolution of the flow. However, there are assumptions about the CFD model currently set up which we have assumed, these assumptions greatly decreases the running time and calculations needed to get an extremely accurate result for one which can be accepted as accurate enough in which the solution is also converging and does not run for a significantly long amount of time. One of these assumptions is the flows laminarity by using a low $Re_D$, by setting up this parameter we have assumed the flow consistency, the fluid particles travel in uniformity with consistent velocities and trajectories, minimal mixing of adjacent layers of the flow which also leads to reduced energy loss between the particles and the boundary wall. In turbulent flows, higher $Re_D$ guarantee chaos of the flow, no longer in layers, leading to inefficient energy going towards the formation of vortices.[11] The limitation of using this model is for a range of different fluid types, the transition between laminar and turbulence varies and if the flow were to be turbulent, there is great velocity and pressure difference which now makes the model ineffective for the relative application where laminar flow is needed.

## 3.5 Flow Transition

As seen in figure 6, experimentally, the transition of laminar and turbulent flow can be identified by observing the gap between the two set of points. It is easy to identify this as they do not follow the linear laminar curve or the turbulent curve and appear as anomalies for the two data. The flow transition occurred at the $Re_D$, $5620 \pm 225$, error calculated from the mean of the readings in which there is an log Re axis error and $C_f$ as $Re_D$ is used within it as in the formula above. Empirically, any $Re_D$ under 2300 is, with great certainty, laminar flow, equally, values over 4000 is turbulent. The value interpreted in the conducted experiment is slightly higher than this however, which can be explained by a multitude of reasons. The primary reason for which the transition is so high is the uniform velocity profile which can delay flow transition by maintaining stable laminar flow conditions downstream. Along with this, the current flow configuration promotes stable laminar flow behaviour making it more resistant to the transition to the turbulent regime, this also means it is under very preferable pressure distributions and the symmetry leads to smoother flow in which it is harder to induce mixing of adjacent layers of the flow.

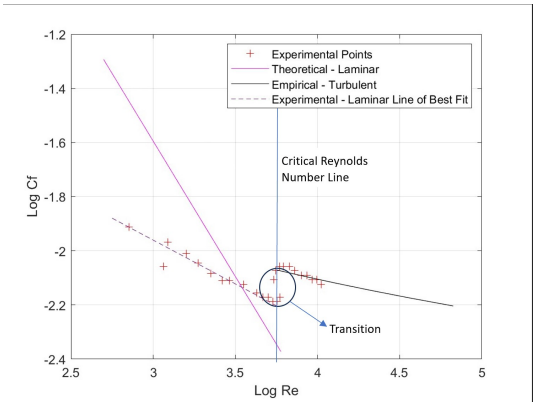


Figure 6: Variation of $C_f$ with $Re_D$ indicating transition from laminar to turbulent flow - error bars removed intentionally to visually see data points

# 4 Conclusions

In conclusion, comparing the results produced by experimental, computational, and theoretical methods for analysing flow through a pipe, several key observations emerge. These observations and data analysed have given quantities, most vital being the skin friction coefficient, of varying accuracy

The experimental method measured manometer readings from the pressure tappings across the perspex pipe which was used in conjunction with a running plot to see the development of flow over time and identify regions of laminar and turbulence. At the end the relative errors in the experimental errors are 26.979% in comparison with the computational for $C_p$ and for the $C_f$ in the laminar region a 70% error and 4.8% error in the turbulent, these agree along the same magnitude with empirical evidence of Hagen and Poiseuille[6] as well as Colebrook and White.[12] These measurements provide precise data under specific conditions but were influenced by experimental uncertainties such as calibration. Additionally, the experimental setup involved practical challenges like ensuring the flow conditions remain consistent throughout the experiment. Despite these challenges, the designed experiments could still offer reliable data for validating and refining computational and theoretical models. If redoing the experiment, close attention will be towards the manometers and flow rate will be properly calibrated, the experiment will also be repeated at least ten more times and anomalies will be identified and excluded from mean calculated.

Computational methods, such as CFD, simulate flow behavior using numerical techniques. The models accurately predicted $C_f$ by solving the Navier-Stokes equations governing fluid flow. These simulations offer a detailed understanding of flow dynamics and provide $C_f$ predictions across a wide range of conditions. However, the accuracy of CFD predictions depends on the fidelity of the model and the computational resources available. Simplifications or approximations in the model can affect the accuracy of the results as well as not having the ability to model turbulent flow according to our model. The computation compared to theory for $C_f$ is 1.778% which, in ideal conditions, is a very suitable accuracy as there will still be some error corresponding to the values retrieved from the Navier-Stokes equation however if conducting again this step could also be repeated ten times and obtain a mean to reduce the uncertainty by ten fold.

Theoretical methods, based on fundamental principles of fluid mechanics, provide analytical expressions for estimating the $C_f$. These expressions are derived from simplified flow assumptions, such as the laminar or turbulent nature of the flow, included empirical correlations. Theoretical models offer simplicity and can be applied to quickly to estimate $C_f$ for various flow conditions. However, they may lack accuracy compared to experimental or computational results as, same with computational methods, assumptions like constant density and incompressible flow had been assumed especially for complex flow regimes or non-ideal geometries. Theoretical values compared to the others should be the most accurate and what it should be but could be even more accurate if considered surface roughness. A range of other $Re_D$ could also be used within CFD to compare the $C_f$ to the theory.

In summary, experimental methods provide precise but limited data, computational methods offer detailed predictions across a wide range of conditions, and theoretical methods offer quick estimates based on simplified assumptions. Each approach has its strengths and limitations when predicting the $C_f$, and a comprehensive analysis often involves comparing and combining results from all three methods to improve accuracy and reliability.

# References


[1] Donald C Rennels. *Pipe flow: A practical and comprehensive guide*. John Wiley & Sons, 2022.

[2] T Cebeci J Cousteix and J Cebeci. Modeling and computation of boundary-layer flows. *Berlin, Germany: Springer*, 2005.

[3] David F Rogers. *Laminar flow analysis*. Cambridge University Press, 1992.

[4] Michael Eckert. Pipe flow: a gateway to turbulence. *Archive for History of Exact Sciences*, 75(3):249–282, 2021.

[5] Derek Jackson and Brian Launder. Osborne reynolds and the publication of his papers on turbulent flow. *Annu. Rev. Fluid Mech.*, 39:19–35, 2007.

[6] Peter W Duck. Transient growth in developing plane and hagen poiseuille flow. *Proceedings of the Royal Society A: Mathematical, Physical and Engineering Sciences*, 461(2057):1311–1333, 2005.

[7] Johann Nikuradse et al. Laws of flow in rough pipes. 1950.

[8] A Abou El-Azm Aly, A Chong, F Nicolleau, and S Beck. Experimental study of the pressure drop after fractal-shaped orifices in a turbulent flow pipe. *World Acad. Sci. Eng. Technol*, 4, 2008.

[9] Rajesh Bhaskaran and Lance Collins. Introduction to cfd basics. *Cornell University-Sibley School of Mechanical and Aerospace Engineering*, pages 1–21, 2002.

[10] Peter Bradshaw. The understanding and prediction of turbulent flow. *The Aeronautical Journal*, 76(739):403–418, 1972.

[11] Francis R Hama, James D Long, and John C Hegarty. On transition from laminar to turbulent flow. *Journal of Applied Physics*, 28(4):388–394, 1957.

[12] Ajinkya A More. Analytical solutions for the colebrook and white equation and for pressure drop in ideal gas flow in pipes. *Chemical engineering science*, 61(16):5515–5519, 2006.

# Appendix

## 4.1 Appendix A: Diagram to aid in visualisation of the model

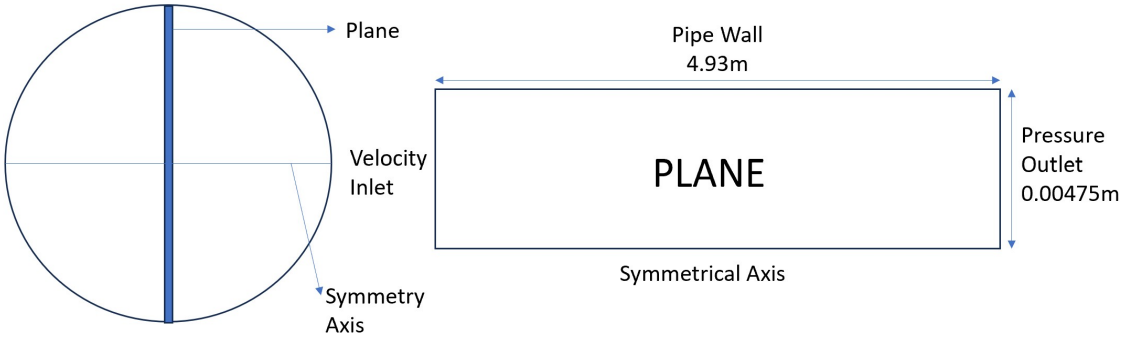

## 4.2 Appendix B: Navier-Stokes Equations

$$\frac{\partial \rho}{\partial t} + \nabla \cdot (\rho \mathbf{u}) = 0, \tag{7}$$

$$\rho \left( \frac{\partial \mathbf{u}}{\partial t} + (\mathbf{u} \cdot \nabla)\mathbf{u} \right) = -\nabla p + \mu \nabla^2 \mathbf{u}, \tag{8}$$

where: $\rho$ =Fluid density,
u=Velocity,
p=pressure,
$\mu$ =Dynamic Viscosity,
f=External body forces,

### 4.3 Appendix C: Link to Detailed Experimental Data

http://tinyurl.com/2eerdbsx

## 4.4 Appendix D: Link to Detailed MATLAB Program

http://tinyurl.com/mrmu3yae